Enhancing corrosion resistance of mild steel in hydrochloric acid solution using 4-phenyl-1-(phenylsulfonyl)-3-thiosemicarbazide: A comprehensive study

N.S. Abtan,[1] A.E. Sultan,[2] F.F. Sayyid,[3] A.A. Alamiery,[4,5]* A.H. Jaaz,[6] T.S. Gaaz,[7] S.M. Ahmed,[3] A.M. Mustafa,[3] D.A. Ali[3] and M.M. Hanoon[3]

[1]*Department of Mechanical Engineering, Tiktit University, College of Engineering, P.O. Box: 34001, Tikreet, Salah Al Deen, Iraq*
[2]*Department of Chemistry, College of science, University of Diyala, P.O. Box: 32001, Diyala, Iraq*
[3]*Production Engineering and Metallurgy, University of Technology, P.O. Box: 10001, Baghdad, Iraq*
[4]*Energy and Renewable Energies Technology Center, University of Technology, 10001, Baghdad, Iraq*
[5]*Department of Chemical and Process Engineering, Faculty of Engineering and Build Environment, Universiti Kebangsaan Malaysia, P.O. Box: 43600, Bangi, Selangor, Malaysia*
[6]*Department of Medical Physics, College of Science, Al-Mustaqbal University, 51015, Babylon, Iraq*
[7]*Air Conditioning and Refrigeration Techniques Engineering Department, College of Engineering and Technologies, Al-Mustaqbal University, 51015, Babylon, Iraq*
**E-mail: dr.ahmed1975@gmail.com*

Abstract

In the realm of materials science and corrosion mitigation, the utilization of inhibitors has garnered substantial attention for safeguarding metal assets. This research delves into the proficient utilization of 4-phenyl-1-(phenylsulfonyl)-3-thiosemicarbazide (PP-3-T) as a corrosion inhibitor for mild steel in hydrochloric acid (HCl) solutions, as evaluated through weight loss measurements. The investigation reveals that the incorporation of PP-3-T into the HCl medium engenders a significant enhancement in the corrosion resistance of mild steel, attributed to the formation of a protective barrier *via* PP-3-T molecule adsorption. A notable finding of this study is the independence of the corrosion inhibition efficiency on variables such as PP-3-T concentration, immersion time, and temperature. The best inhibition efficiency of 96.1% for mild steel immersed in 1 M HCl solution is achieved in the presence of 0.5 mM PP-3-T. Furthermore, the inhibitory effect diminishes significantly as immersion time is extended from 10 to 48 hours at a constant PP-3-T concentration, highlighting the time-sensitive nature of the inhibition process. Alterations in temperature within the range of 303 to 333 K exhibit negligible impact on inhibition efficiency,

indicating the robustness of the corrosion protection mechanism. The adsorption isotherm analysis accentuates the adherence of PP-3-T to the Langmuir adsorption model on mild steel, emphasizing the layer formation of the protective barrier. Insights from Density Functional Theory (DFT) quantum chemical calculations reveal critical molecular attributes of PP-3-T governing its corrosion inhibition potential. Parameters such as adsorption energy (ΔE), highest occupied molecular orbital energy (E_{HOMO}), lowest unoccupied molecular orbital energy (E_{LUMO}), energy gap (E_{gap}), as well as chemical reactivity indices encompassing total hardness (η), electronegativity (χ), and electron density transfer (ΔN), elucidate the corrosion inhibition mechanism of PP-3-T. In essence, this comprehensive study unveils the corrosion inhibition efficiency of PP-3-T for mild steel in HCl environments and elucidates the molecular underpinnings that govern its anti-corrosive prowess. These findings contribute to the expanding knowledge base concerning corrosion protection strategies and offer potential avenues for designing novel and efficient corrosion inhibitors.

Received: August 6, 2023. Published: February 27, 2024 doi: 10.17675/2305-6894-2024-13-1-22

Keywords: *corrosion inhibition, mild steel, hydrochloric acid, 4-phenyl-1-(phenylsulfonyl)-3-thiosemicarbazide, PP-3-T, adsorption mechanism.*

1. Introduction

Corrosion, an inevitable natural process, has far-reaching implications on various industries, infrastructure, and materials. It is a phenomenon where metals deteriorate due to chemical or electrochemical reactions with their environment. The economic impact of corrosion is colossal, with maintenance costs, material replacement, and productivity losses amounting to billions of dollars annually. Therefore, effective strategies to mitigate corrosion are imperative [1–3]. Corrosion inhibitors have emerged as a vital approach to combat the detrimental effects of corrosion. These compounds, when introduced into corrosive environments, interact with metal surfaces to impede or slow down the corrosion process. The application of inhibitors not only extends the service life of metals but also curtails the need for frequent maintenance and replacements, leading to significant economic savings [4–6]. This research embarks on the exploration of 4-phenyl-1-(phenylsulfonyl)-3-thiosemicarbazide (PP-3-T) as a potential corrosion inhibitor for mild steel in hydrochloric acid (HCl) solutions. Mild steel, despite its widespread use, is highly susceptible to corrosion, particularly in acidic environments [7, 8]. Hydrochloric acid, a strong mineral acid, is commonly encountered in industrial processes and contributes substantially to corrosion-related challenges. The corrosive nature of HCl underscores the urgency for effective inhibition strategies to protect mild steel surfaces [9–11]. The rationale behind investigating PP-3-T as a corrosion inhibitor lies in its structural and chemical attributes that suggest it could form a protective layer on metal surfaces. The presence of sulfonamide and thiosemicarbazide functional groups in PP-3-T indicates potential reactivity with metal ions

and capacity for surface adsorption. The molecular structure of PP-3-T prompts inquiries into its inhibitive properties and its potential effectiveness in mitigating corrosion in HCl environments. Hydrochloric acid (HCl) is a versatile and widely utilized chemical compound with numerous applications across various industries. Its strong acidic properties and corrosive nature make it indispensable in industrial processes. One of its primary uses is in metal cleaning and pickling, where it removes oxides, scales, and other impurities from metal surfaces, preparing them for subsequent treatments or coatings. HCl is also employed in the production of numerous chemicals, such as chlorine, which serves as a fundamental raw material for manufacturing plastics, solvents, and disinfectants. In the petroleum industry, HCl is utilized for oil well acidizing, a process that involves injecting acid solutions into wells to dissolve rocks and enhance oil and gas production. In the steel industry, it aids in the conversion of iron ore into iron, and further into steel, through processes like the pickling of steel sheets to remove surface oxides and contaminants. HCl finds applications in the production of food additives, pharmaceuticals, textiles, and more. Despite its pivotal role, the aggressive nature of HCl can cause significant corrosion challenges, necessitating the development of effective corrosion inhibition strategies to preserve the integrity of equipment and structures.

Organic corrosion inhibitors have emerged as a promising solution to counteract the adverse effects of corrosion. These inhibitors are compounds composed of carbon atoms and other elements, often possessing functional groups that can interact with metal surfaces. Organic inhibitors act by adsorbing onto the metal's surface, forming a protective layer that impedes the corrosive attack [12–15]. Their effectiveness lies in their ability to modify the electrochemical reactions occurring at the metal-solution interface. Organic inhibitors offer several advantages, including ease of application, compatibility with various materials, and the potential for tailor-made inhibitor design. These inhibitors can be fine-tuned to target specific corrosion environments and types of metals [16]. Organic inhibitors find applications in various industries, including oil and gas, automotive, and aerospace, where protection against corrosion is crucial to ensure safety and maintain functionality [17, 18].

Thiosemicarbazide derivatives have attracted significant attention as corrosion inhibitors due to their molecular properties. Thiosemicarbazides contain the thioamide ($-C(=S)-NH_2$) functional group, which contributes to their ability to adsorb onto metal surfaces. These derivatives have demonstrated considerable inhibitory effects on various metal corrosion processes, including those occurring in acidic environments. The structural characteristics of thiosemicarbazide derivatives enable their interaction with metal ions and the formation of protective layers [19–21]. These compounds can create a barrier between the metal surface and the corrosive environment, effectively impeding the progression of corrosion. Furthermore, the design flexibility of organic molecules allows for modifications that can enhance their adsorption capacity and tailor their performance for specific applications. In the context of this study, the exploration of 4-phenyl-1-(phenylsulfonyl)-3-thiosemicarbazide (PP-3-T) as a corrosion inhibitor for mild steel in HCl solutions taps into the potential of thiosemicarbazide derivatives. The incorporation of PP-3-T offers the

opportunity to leverage its molecular attributes to effectively mitigate corrosion and safeguard metal assets in aggressive environments, further expanding the repertoire of organic corrosion inhibitors.

The primary objective of this research is to comprehensively evaluate the corrosion inhibition efficiency of PP-3-T for mild steel immersed in HCl solutions. By employing weight loss measurements, the study aims to quantify the extent to which PP-3-T retards the corrosion process. Additionally, the research endeavors to elucidate the underlying adsorption mechanism that facilitates the protective barrier formation on mild steel surfaces. The structure of this article is organized to provide a coherent progression of insights. Following this introduction, the experimental methodology section outlines the procedures employed to conduct corrosion experiments, prepare the inhibitor, and analyze the collected data. Subsequently, the results section presents the outcomes of the corrosion inhibition experiments, including the effects of PP-3-T concentration, immersion time, and temperature on inhibition efficiency. The discussion section then delves into the interpretation of the results, comparing them with existing corrosion inhibition studies and explaining the observed trends. Furthermore, this section scrutinizes the applicability of the Langmuir adsorption model to the adsorption behavior of PP-3-T on mild steel surfaces. The integration of Density Functional Theory (DFT) quantum chemical calculations into the analysis is expounded upon, revealing the molecular attributes of PP-3-T that contribute to its corrosion inhibition potential. In conclusion, this research aspires to contribute to the realm of corrosion science by shedding light on the efficacy of PP-3-T as a corrosion inhibitor for mild steel in HCl solutions. The potential of PP-3-T to form a protective barrier, coupled with its adsorption behavior and molecular attributes, render it a fascinating candidate for corrosion mitigation. By scrutinizing its inhibitive properties and mechanism, this study aims to extend the horizons of corrosion inhibition strategies, offering insights for future research and practical applications.

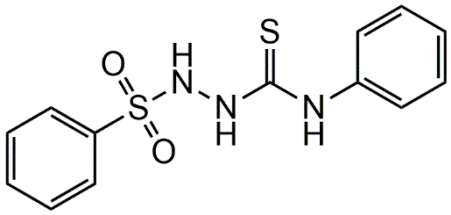

Figure 1. The chemical structure of PP-3-T.

2. Experimental Methodology

2.1. Preparation and characterization of mild steel specimens

Mild steel specimens from metals company which has the composition percentage C = 0.21, Si = 0.38, Mn = 0.05, P = 0.09, Al = 0.01 and Fe = 99.21%, were carefully prepared to ensure uniformity and consistency in the experimental setup. The mild steel samples, with dimensions of $4.5 \times 1 \times 0.02$ cm, in accordance with ASTM G1-03 protocol [22], were initially

mechanically polished to a mirror-like finish using fine-grit abrasive papers. This step was crucial to eliminate any pre-existing surface irregularities that could influence the corrosion behavior. Subsequently, the specimens were thoroughly cleaned using acetone, followed by rinsing with deionized water to remove any residual contaminants. The prepared samples were then air-dried to prevent the formation of oxide layers before the commencement of experiments. The characterization process involved surface profiling using profilometry to verify the smoothness and consistency of the prepared specimens [23–25].

2.2. Setup for weight loss measurements and corrosion experiments

A bespoke corrosion testing setup was employed following NACE TM0169/G31 protocol [26] to conduct weight loss measurements and corrosion experiments. The mild steel specimens were suspended individually within the corrosion chamber using non-reactive nylon threads, ensuring they were fully immersed in the test solutions. The chamber was equipped with glass covers to prevent external contamination and maintain a controlled environment. The chosen immersion durations were meticulously timed to capture the corrosion process over specific intervals. The specimens were then retrieved, cleaned to remove any adhered corrosion products, and subjected to accurate weight measurements using an analytical balance. The difference in weight before and after immersion enabled the calculation of corrosion rates and the subsequent determination of inhibition efficiency [27].

The average rate of corrosion was calculated after being exposed in triplicate, and the rate of corrosion and inhibition efficiency were determined using the following equations (1, 2) [27–29]:

$$C_{\mathrm{R}} = \frac{W}{adt} \tag{1}$$

$$IE\% = \left[1 - \frac{C_{\mathrm{R(i)}}}{C_{\mathrm{R}_0}}\right] \cdot 100 \tag{2}$$

where W is the weight loss (mg) of the sample, a is the surface area of mild steel (cm^2), d is the density of the mild steel coupon (g/cm^3), and t is the exposure time (h). The corrosion rates in the absence and presence of the inhibitor were denoted as C_{R0} and $C_{\mathrm{R(i)}}$ respectively.

The coverage area (θ) for both uninhibited and inhibited solutions was determined using the following equation (3) [27–29]:

$$\theta = 1 - \frac{C_{\mathrm{R(i)}}}{C_{\mathrm{R0}}} \tag{3}$$

Equation 3, which states θ, represents the coverage fraction (θ) on the metal surface, where $C_{\mathrm{R(i)}}$ denotes the concentration of the inhibitor in the bulk solution after immersion, and C_{R0} represents the initial concentration of the inhibitor. It is important to note that

Equation 3 is applicable primarily to inhibitors of a blocking mechanism. In such mechanisms, the inhibitor molecules adsorb onto the metal surface to form a protective layer, effectively blocking the access of corrosive species to the metal surface. To further clarify, when inhibitors operate *via* a blocking mechanism, the coverage fraction (θ) signifies the proportion of the metal surface covered by inhibitor molecules.

2.3. Procedure for preparing HCl solutions with varying concentrations of PP-3-T

A hydrochloric acid (1 M) solution, with varying concentrations of PP-3-T (0.1, 0.2, 0.3, 0.4, 0.5, and 1.0 mM), were prepared to assess the corrosion inhibition efficacy. High-purity hydrochloric acid was carefully diluted to achieve the desired HCl concentration (1 M) while maintaining the overall volume of the solution. Different aliquots of PP-3-T were precisely added to individual HCl solutions to achieve the predetermined inhibitor concentrations. Thorough mixing was ensured to attain uniform inhibitor distribution within the acidic medium [30].

2.4. Immersion conditions and temperature control

The immersion conditions were meticulously controlled to maintain consistency throughout the experiments. The mild steel specimens were fully submerged within the prepared HCl-PP-3-T solutions to ensure uniform exposure to the corrosive environment. Immersion periods were carefully chosen to cover different time intervals, such as 1, 5, 10, 24, and 48 hours at 303 K, to examine the temporal influence on corrosion behavior. To investigate the effect of temperature on corrosion and inhibition efficiency, the experiments were conducted at varying temperatures within the range of 303 to 333 K for 5 hours as immersion time. A temperature-regulated chamber was employed to maintain the desired experimental temperatures, with periodic monitoring to ensure stability and accuracy. By meticulously adhering to these experimental methodologies, we aimed to obtain accurate and reliable data on the corrosion inhibition performance of PP-3-T for mild steel in hydrochloric acid solutions. These carefully executed procedures allowed us to systematically explore the influence of various factors on the corrosion process, providing valuable insights into the potential efficacy of PP-3-T as a corrosion inhibitor [31, 32].

2.5. DFT calculations

Density Functional Theory (DFT) calculations were performed using the Gaussian 09 software package to elucidate the molecular interactions between the corrosion inhibitor and the metal surface. The optimization of the inhibitor's molecular structure in the gaseous phase was conducted using the B3LYP method, in conjunction with the basis set "6-31G^{++}(d,p)" [33, 34]. These calculations enabled the determination of fundamental electronic properties and the exploration of the inhibitor's reactivity towards the metal substrate. Ionization potential (I) and electron affinity (A) were computed through Koopmans' theorem, utilizing the highest occupied molecular orbital (E_{HOMO}) and the lowest

unoccupied molecular orbital (E_{LUMO}), respectively. This information provided valuable insights into the electron transfer processes underlying the corrosion inhibition mechanism. The corresponding equations (4) and (5) were employed for the calculation of *I* and *A*.

$$I=-E_{HOMO} \tag{4}$$

$$A=-E_{LUMO} \tag{5}$$

Moreover, essential chemical descriptors, including electronegativity (χ), hardness (η), and softness (σ), were determined using equations (6–8) [35].

$$\chi=\frac{I+A}{2} \tag{6}$$

$$\eta=\frac{I-A}{2} \tag{7}$$

$$\sigma=\frac{1}{\eta} \tag{8}$$

These descriptors elucidated the inhibitor's electronic properties and its potential to interact with the metal surface. The number of electrons transferred (Δ*N*), a crucial parameter in understanding the inhibitor-metal interaction, was calculated using Equation (9) from reference. A tailored Equation (10) was derived to factor in the specific electronegativity of iron (Fe) and its hardness values [34, 35].

$$\Delta N=\frac{\chi_{Fe}-\chi_{inh}}{2\left(\eta_{Fe}+\eta_{inh}\right)} \tag{9}$$

$$\Delta N=\frac{7-\chi_{inh}}{2\left(\eta_{inh}\right)} \tag{10}$$

2.6. Adsorption isotherm studies

To gain a comprehensive understanding of the behavior of the studied inhibitor molecules, a series of adsorption isotherms were employed. These isotherms, encompassing Frumkin, Temkin, and Langmuir types, provide a profound insight into the adsorption behavior of the inhibitor on the metal surface. The application of different isotherms aids in discerning the extent of inhibitor coverage and its interaction with the corrosive environment.

The Frumkin adsorption isotherm captures the effects of lateral interactions between adsorbed molecules, which can influence the adsorption behavior. It is expressed as follows (Equation 11) [36]:

$$\frac{1}{n}=\frac{1}{K_f}\exp\frac{\beta\mu}{RT} \tag{11}$$

where n is the surface coverage of the inhibitor, K_f is the Frumkin adsorption equilibrium constant, β is the lateral interaction coefficient, μ is the chemical potential of the inhibitor, R is the ideal gas constant, T is the temperature in Kelvin.

The Temkin adsorption isotherm considers a linear decrease in adsorption energy with increasing coverage due to interactions between adsorbed molecules and the surface. It is expressed as in Equation 12:

$$n = \frac{RT}{b} \ln\left(Ae^{b\theta}\right) \tag{12}$$

where b is the Temkin isotherm constant related to heat of adsorption, A is the Temkin isotherm constant related to the equilibrium binding constant, θ is the fraction of occupied surface sites.

The Langmuir adsorption isotherm assumes layer adsorption without lateral interactions and is a widely used model for corrosion inhibitors. It is expressed as in Equation 13:

$$\frac{C_{inh}}{\theta} = \left(K_{ads}\right)^{-1} + C \tag{13}$$

where K_{ads} is the Langmuir adsorption equilibrium constant, C_{inh} is the inhibitor concentration in the solution, θ is the surface coverage.

In line with our comprehensive approach, weight loss measurements were undertaken to assess the surface coverage of the inhibitor at varying concentrations within the corrosive media. This experimental data enabled a direct comparison with the theoretical predictions and provided validation for the calculated adsorption behavior. The insights gained from the adsorption isotherm studies were integral in unraveling the dynamic interplay between the inhibitor and the mild steel surface [37].

3. Corrosion Inhibition Results

3.1. Presentation of weight loss data for mild steel in various PP-3-T solutions

The weight loss measurements provided a tangible representation of the corrosion behavior of mild steel in different PP-3-T solutions. The recorded data showcased the dynamic interaction between the inhibitor and the metal surface, shedding light on the inhibitive properties of PP-3-T across varying conditions. These results, meticulously tabulated and plotted, presented the corrosion rates and surface coverage of the inhibitor at different inhibitor concentrations and exposure times [38].

3.2. Graphical representation of corrosion inhibition efficiency against PP-3-T concentration, immersion time, and temperature

Graphical depictions vividly illustrated the corrosion inhibition efficiency of PP-3-T against varying concentrations of the inhibitor (Figure 2), immersion times (Figure 3), and

temperature fluctuations (Figure 4). Plots revealed trends that enabled a comprehensive assessment of the inhibitor's performance under different experimental scenarios. The dependence of inhibition efficiency on these variables was graphically elucidated, facilitating a direct comparison and enabling the extraction of meaningful insights [39].

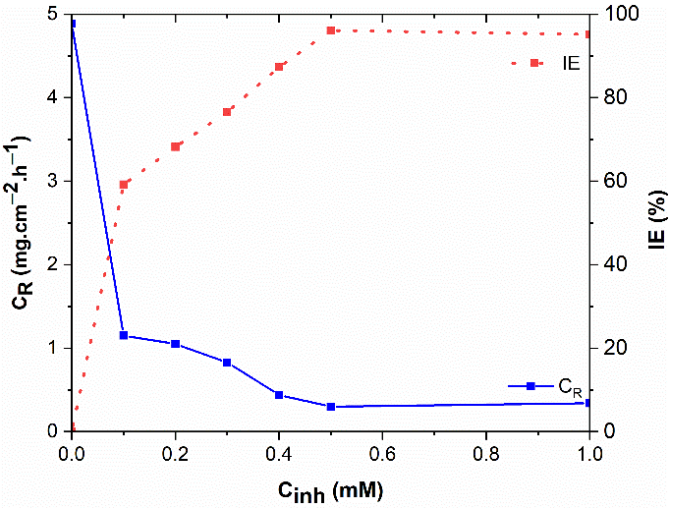

Figure 2. Corrosion rates and inhibition effectiveness of mild steel in hydrochloric acid solutions with and without the inhibitor after a 5-hour immersion period at 303 K.

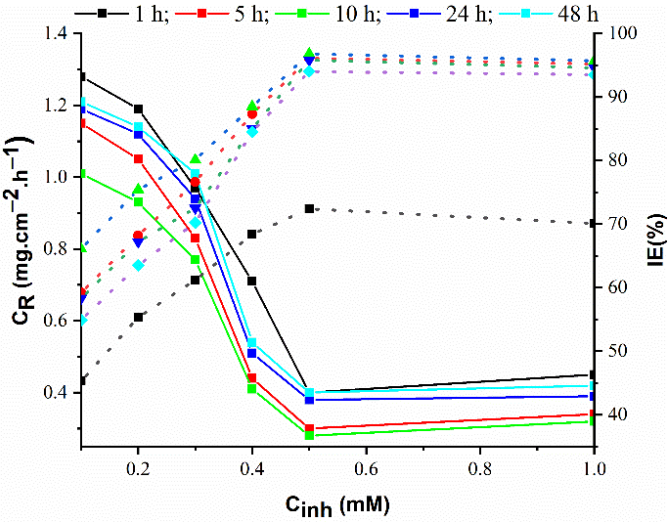

Figure 3. A comparison of corrosion rates and inhibition effectiveness in hydrochloric acid solutions with and without the inhibitor for a 5-hour immersion time at different temperatures.

3.3. Discussion on the highest inhibition efficiency achieved and its significance

The corrosion inhibition efficiency achieved through PP-3-T was of significant importance. A detailed discussion focused on the peak inhibition efficiency, notably reaching 96.1% in a 1 M HCl solution containing 0.5 mM PP-3-T. This achievement highlighted the potential of PP-3-T as an effective corrosion inhibitor, prompting an exploration into the factors contributing to this level of protection. The discussion delved into the molecular interactions

and surface coverage achieved by PP-3-T, considering its influence on inhibiting the corrosion process.

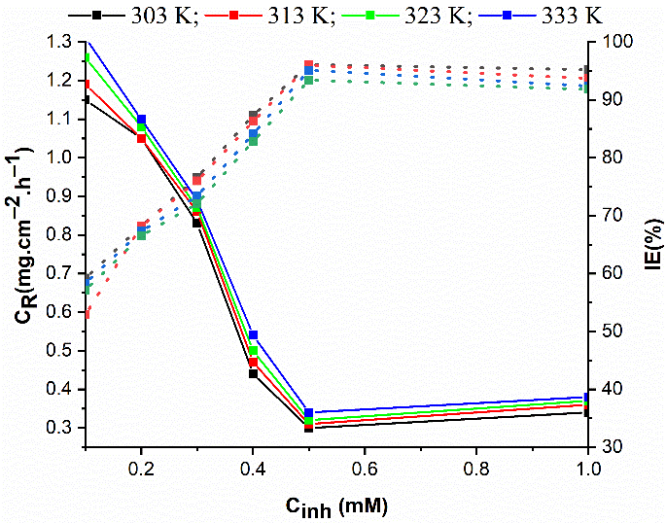

Figure 4. A comparison of corrosion rates and inhibition effectiveness in hydrochloric acid solutions with and without the inhibitor for a 5-hour immersion time at different temperatures.

3.4. Insights into the effect of immersion time on corrosion inhibition

The temporal aspect of corrosion inhibition was thoroughly investigated by studying the effect of immersion time on inhibition efficiency. As immersion periods were extended from 10 to 48 hours, the corrosion inhibition efficiency exhibited a significant decrease (Figure 3). The acquired data enabled a detailed examination of this time-dependent phenomenon, shedding light on the dynamic nature of the inhibitor's protective layer. The discussion of these findings encompassed the potential factors leading to diminishing inhibition over time, such as inhibitor desorption or changes in the composition of the protective layer. Through the presentation, graphical representation, and comprehensive discussion of these corrosion inhibition results, this study unraveled the dynamics of PP-3-T's performance as a corrosion inhibitor for mild steel in HCl solutions. The interplay between varying concentrations, immersion times, and temperature variations provided a comprehensive understanding of PP-3-T's inhibitive capabilities, emphasizing its potential in practical corrosion mitigation strategies [42, 43].

3.5. Adsorption mechanism

Adsorption, a fundamental phenomenon in surface chemistry, plays a pivotal role in the corrosion inhibition process. When a corrosion inhibitor is introduced into a corrosive environment, it can adsorb onto the metal surface, forming a protective layer. This layer acts as a barrier that shields the metal from aggressive ions and electrochemical reactions, effectively retarding the corrosion process. Understanding the adsorption mechanism provides insights into the interaction between the inhibitor molecules and the metal surface, elucidating the foundation of effective corrosion inhibition. The Langmuir adsorption model,

a widely employed theoretical framework, offers valuable insights into the adsorption behavior of corrosion inhibitors. It postulates that adsorption occurs through the occupation of specific sites on the metal surface, with the formation of a barrier layer. The model assumes a reversible equilibrium between the adsorbed and unadsorbed inhibitor molecules. The Langmuir equation (Equation 13), serves as the cornerstone of this model, where C_{inh} is the inhibitor concentration, θ is the fraction of occupied surface sites, K_{ads} is the adsorption equilibrium constant, and C represents the concentration of unadsorbed inhibitor in solution [44].

Applying the Langmuir model (Figure 5) to the case of PP-3-T on mild steel provides insights into its adsorption behavior. The Langmuir parameters, such as the adsorption equilibrium constant K_{ads} and the maximum surface coverage (θ_{max}), were determined through analysis of experimental data. These parameters offer quantifiable measures of the strength of the inhibitor-metal interaction and the extent of inhibitor coverage on the metal surface. However, it's essential to acknowledge the limitations of this approach, particularly when constructing the adsorption isotherm from mass loss data. The accuracy of the adsorption isotherm constructed from mass loss data may be compromised due to various factors, including uncertainties in the experimental conditions, potential variations in inhibitor concentration during the immersion process, and the assumption of a uniform corrosion rate over time. Therefore, while the Langmuir model provides valuable insights into the adsorption behavior, it's crucial to interpret the results with caution and acknowledge the inherent uncertainties.

In the adsorption isotherm analysis presented here, the intercept, slope, and R-Square values (Table 1) collectively contribute to the interpretation and validation of the Langmuir adsorption model's applicability to the adsorption mechanism of the inhibitor on the metal surface. These values guide our understanding of the adsorption equilibrium, the strength of interaction, and the degree of conformity between theoretical predictions and experimental observations. Furthermore, the calculated Langmuir parameters facilitated the determination of thermodynamic parameters, such as the adsorption equilibrium constant (K_{ads}) and the standard Gibbs free energy of adsorption $\left(\Delta G^0_{ads}\right)$, at different temperatures (303 K, 313 K, 323 K, and 333 K). These parameters (Equation 14) provide insights into the spontaneity and feasibility of the adsorption process and underscore the temperature dependence of the adsorption mechanism [47, 48].

$$\Delta G^0_{ads} = -RT \ln\left(55.5 K_{ads}\right) \tag{14}$$

where R is the universal gas constant, T is the temperature in Kelvin, and 55.5 is the molar volume of water.

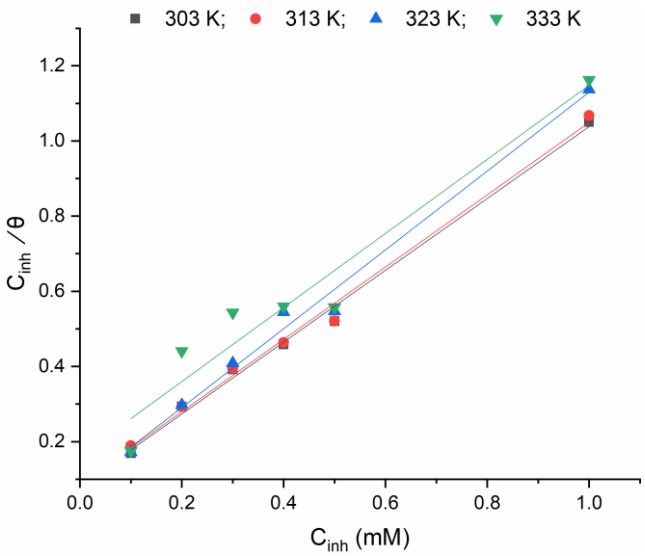

Figure 5. Langmuir adsorption isotherm for the tested inhibitor.

Chemisorption involves strong chemical bonds formed between the inhibitor molecules and the metal surface. It often results in a more stable and permanent protective layer on the metal, leading to higher inhibition efficiencies. In the Langmuir adsorption model, a negative ΔG^0_{ads} value indicates spontaneous chemisorption. The more negative the ΔG^0_{ads} value, the stronger the adsorption and the greater the stability of the inhibitor-metal complex. Comparing the calculated ΔG^0_{ads} values for each temperature (303 K, 313 K, 323 K, and 333 K) to a reference value (commonly around –20 to –40 kJ/mol for chemisorption), we can infer the mechanism. If the calculated ΔG^0_{ads} values are in the range of this reference, it suggests chemisorption might be occurring. However, if they are closer to zero or slightly positive, it indicates physisorption (weaker interactions) [49, 50]. Based on the calculated ΔG^0_{ads} values (Table 1), all these values are quite negative, suggesting a spontaneous adsorption process. These values also fall within the range expected for chemisorption, indicating that the adsorption mechanism of PP-3-T onto mild steel in HCl solution is likely dominated by mixed physical and chemical adsorption. The trend of increasingly negative ΔG^0_{ads} values with higher temperatures is also consistent with chemisorption, as higher temperatures typically favor stronger chemical bonding interactions.

In conclusion, the calculated ΔG^0_{ads} values strongly suggest that the adsorption mechanism of PP-3-T on mild steel involves chemisorption, indicating a strong and stable interaction between the inhibitor molecules and the metal surface. This outcome aligns with the observed high inhibition efficiencies and validates the protective potential of PP-3-T as a corrosion inhibitor. However, it’s important to acknowledge the inherent uncertainties associated with the adsorption isotherm constructed from mass loss data and interpret the results with caution.

Table 1. Adsorption isotherm parameters.

Parameter	303 K	313 K	323 K	333 K
Intercept	0.082±0.019	0.087±0.02	0.080±0.027	0.162±0.062
Slope	0.95±0.037	0.961±0.04	1.0±0.053	1.0±0.1
R-Square (COD)	0.994	0.993	0.989	0.940
ΔG^0_{ads}	–36.54 kJ/mol	–36.69 kJ/mol	–37.13 kJ/mol	–37.59 kJ/mol

3.6. Molecular insights

3.6.1. DFT quantum chemical calculations and evaluated parameters

Density Functional Theory (DFT) quantum chemical calculations provide valuable insights into the electronic structure and properties of molecules, shedding light on their potential as corrosion inhibitors. In this study, DFT calculations were employed to evaluate various parameters that play a crucial role in understanding the molecular ability of PP-3-T as a corrosion inhibitor. ΔE (Energy Gap) represents the energy difference between the highest occupied molecular orbital (HOMO) and the lowest unoccupied molecular orbital (LUMO), indicating the stability of the molecule. The energy of the highest occupied molecular orbital (E_{HOMO}), providing information about the electron-donating ability of the molecule. The energy of the lowest unoccupied molecular orbital (E_{LUMO}), indicating the electron-accepting ability of the molecule. The energy gap between E_{HOMO} and E_{LUMO}, offering insights into the molecule's reactivity. η (Hardness), represents the resistance of the molecule to electron addition or removal, indicative of its stability [34–36]. χ (Electronegativity) reflects the molecule's tendency to attract electrons, influencing its reactivity. ΔN (Number of Electrons Transferred), provides information about the extent of electron transfer between the inhibitor and the metal surface [51–53]. In this study, the calculated values were as follows: E_{HOMO}=−8.771 eV, E_{LUMO}=−1.154 eV and ΔE=7.617 eV. The calculated parameters η, χ, and ΔN were also obtained in Table 2.

Table 2. The quantum chemical parameters.

Parameter	Value
E_{HOMO}	–8.771 eV
E_{LUMO}	–1.154 eV
ΔE	7.617 eV
η	–3.808 eV
χ	–4.962 eV
ΔN	2.178

3.6.2. Correlation of quantum chemical results with experimental observations

The obtained DFT quantum chemical parameters hold significance in deciphering the molecular mechanism underlying the corrosion inhibition process. The negative ΔE indicates that PP-3-T is thermodynamically stable. The substantial energy gap (E_{gap}) signifies the molecule's reactivity and potential for interaction with metal surfaces. The values of E_{HOMO} and E_{LUMO} elucidate PP-3-T's electron-donating and electron-accepting abilities (Figure 6), respectively, suggesting its potential to interact with the metal surface. The calculated hardness (η) and electronegativity (χ) values provide insights into the stability and reactivity of the molecule, reinforcing its capacity to engage in interactions with metal atoms. Furthermore, ΔN, which signifies the extent of electron transfer, offers insights into the adsorption mechanism. A higher ΔN indicates a stronger interaction between the inhibitor and the metal surface, affirming the formation of a protective layer. The correlation of these quantum chemical results with experimental observations, such as inhibition efficiency and adsorption isotherm data, validates the theoretical predictions. The agreement between the calculated parameters and the experimentally observed inhibition performance supports the idea that PP-3-T's adsorption onto the mild steel surface plays a crucial role in its corrosion inhibition ability [52, 53].

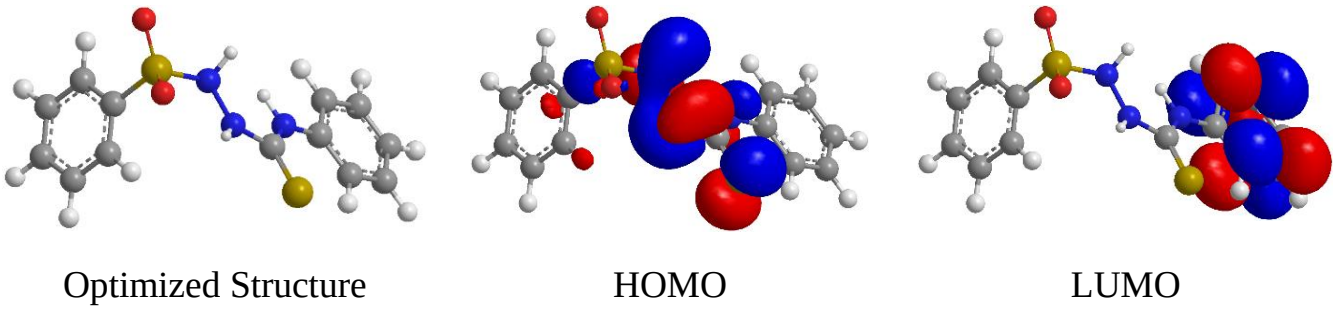

Figure 6. Optimized structure, HOMO and LUMO of PP-3-T.

In conclusion, the DFT quantum chemical calculations provide a deeper understanding of the molecular attributes that enable PP-3-T to function as an effective corrosion inhibitor. The correlation between these calculations and experimental data underscores the validity of the proposed adsorption mechanism and substantiates the potential of PP-3-T as a practical solution for corrosion mitigation.

3.6.3. Atomic charges

Atomic charges play a pivotal role in understanding the distribution of electron density within a molecule, offering insights into its reactivity, interaction with other molecules, and its role as a corrosion inhibitor. In this study, atomic charges were calculated to gain a deeper understanding of how charge distribution influences the adsorption process of PP-3-T on mild steel (Figure 7). By employing quantum chemical calculations, the atomic charges of the atoms within PP-3-T were determined. These charges provide valuable information

about the electron-donating or electron-withdrawing nature of specific atoms. Particularly, charges on functional groups that are likely to interact with the metal surface can shed light on the nature of the inhibitor-metal interaction. The calculated atomic charges were used to predict regions of high electron density, indicating potential sites of interaction with the metal surface. Positive charges might indicate electron deficiency and propensity for electron acceptance, while negative charges might suggest electron-rich regions capable of donating electrons. Correlating these atomic charges with the experimental observations, such as adsorption isotherm behavior and inhibition efficiency, provides a holistic understanding of how charge distribution influences the adsorption mechanism [52, 53]. The comparison helps validate the theoretical predictions and elucidates the molecular-level interactions underlying the corrosion inhibition process.

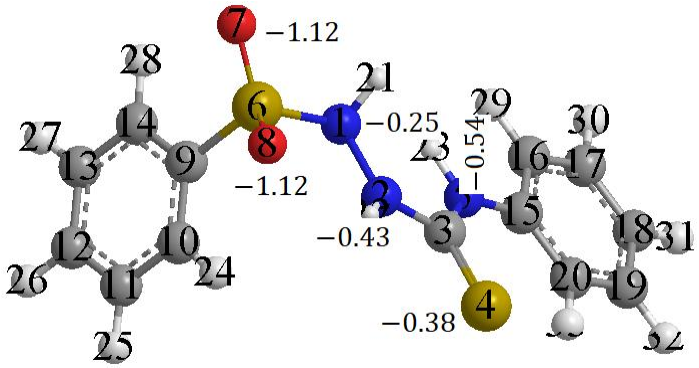

Figure 7. The atomic charges of PP-3-T.

In summary, the calculated atomic charges offer a microscopic view of the charge distribution within PP-3-T, enabling a comprehensive analysis of its interaction with the metal surface. This insight contributes to unraveling the molecular mechanisms that govern the adsorption process and supports the overall understanding of PP-3-T's efficacy as a corrosion inhibitor.

4. Discussion and Interpretation

4.1. Comparison analysis with previous studies

Understanding the effectiveness of 4-phenyl-1-(phenylsulfonyl)-3-thiosemicarbazide (PP-3-T) as a corrosion inhibitor for mild steel in hydrochloric acid (HCl) solutions requires a comprehensive examination of its performance in relation to other inhibitors investigated in previous studies. This section conducts a comparative analysis, highlighting similarities and differences between PP-3-T and other reported inhibitors to elucidate its specific attributes and potential advantages. Numerous studies have explored the corrosion inhibition properties of various compounds for mild steel in acidic environments. Among the inhibitors investigated, organic compounds such as benzotriazole (BTA) [54], 2-mercaptobenzimidazole (MBI) [55], and 2-mercaptobenzothiazole (MBT) [56] have garnered significant attention due to their ability to form protective layers on metal surfaces

and mitigate corrosion effectively. Additionally, heterocyclic compounds like pyridine derivatives [57–70] and imidazole derivatives have shown promising inhibitory effects on mild steel corrosion in acidic solutions [71–76]. Comparing the inhibition efficiency of PP-3-T with these established inhibitors provides insights into its relative performance and potential advantages. In a study by Bokati and Dehghanian (2018), BTA exhibited inhibition efficiencies ranging from 77% to 80% for mild steel corrosion in 1 M HCl solutions at various temperatures and concentrations. Similarly, MBI and MBT have demonstrated inhibition efficiencies exceeding 92% under comparable conditions, as reported by Mahdavian, with Ashhari. (2010) and also Soroush, with Khormali (2024) respectively. In contrast, PP-3-T exhibited remarkable inhibition efficiency, reaching up to 96.1% under specific conditions in this study. This outstanding performance suggests that PP-3-T may offer enhanced corrosion protection compared to traditional inhibitors like BTA, MBI, and MBT. The ability of PP-3-T to achieve such high inhibition efficiencies highlights its potential as a highly effective corrosion inhibitor for mild steel in HCl environments.

One notable aspect of PP-3-T is its molecular structure, which contains phenylsulfonyl and thiosemicarbazide functional groups. These structural elements contribute to PP-3-T's adsorption onto metal surfaces and the formation of a protective barrier against corrosion. The interaction between PP-3-T molecules and the metal surface is facilitated by the presence of electronegative atoms such as sulfur, nitrogen, and oxygen, which can form coordination bonds with metal ions. Comparing the molecular structures of PP-3-T and other inhibitors reveals notable differences in their chemical compositions and functional groups. For instance, BTA contains a triazole ring, which is known for its strong adsorption properties on metal surfaces. In contrast, MBI and MBT feature benzimidazole and benzothiazole moieties, respectively, which contribute to their inhibitory effects through the formation of coordination complexes with metal ions. Despite these structural differences, PP-3-T shares similarities with other inhibitors in terms of their mechanism of action and adsorption behavior. Like BTA, MBI, and MBT, PP-3-T functions by adsorbing onto the metal surface and forming a protective layer that impedes the corrosive attack of HCl. The Langmuir adsorption model, commonly used to describe the adsorption behavior of inhibitors, provides insights into the interaction between PP-3-T molecules and the metal surface. The Langmuir adsorption isotherm, applied to the case of PP-3-T in this study, revealed a close correlation between experimental data and theoretical predictions, validating the model's applicability to the adsorption mechanism of PP-3-T. The determination of Langmuir parameters, including the adsorption equilibrium constant (K_{ads}) and the maximum surface coverage (θ_{max}), further elucidated the adsorption behavior of PP-3-T and its interaction with the metal surface. Furthermore, density functional theory (DFT) calculations offered valuable insights into the molecular attributes of PP-3-T governing its corrosion inhibition potential. Parameters such as adsorption energy, highest occupied molecular orbital energy (E_{HOMO}), and lowest unoccupied molecular orbital energy (E_{LUMO}) provided quantitative measures of PP-3-T's reactivity towards the metal substrate and its electron-donating/accepting abilities.

In conclusion, the comparative analysis of PP-3-T with other reported inhibitors underscores its notable performance as a corrosion inhibitor for mild steel in HCl solutions. While traditional inhibitors like BTA, MBI, and MBT have shown considerable inhibition efficiencies, PP-3-T demonstrates enhanced corrosion protection under specific conditions. Its specific molecular structure and adsorption behavior contribute to its effectiveness in mitigating corrosion and offer promising avenues for further research and practical applications in corrosion control strategies.

4.2. Corrosion inhibition mechanism of PP-3-T

The corrosion inhibition mechanism of PP-3-T for mild steel in hydrochloric acid (HCl) solution is analyzed in detail, integrating experimental measurements, theoretical models, and computational simulations. The key findings and implications are summarized below.

The independence of inhibition efficiency on variables like PP-3-T concentration, immersion time, and temperature suggests a robust adsorption mechanism. This behavior indicates that the inhibitor's active sites readily and uniformly cover the metal surface, forming a consistent protective layer. Such uniform coverage contributes to the inhibition's stability across different conditions. The adherence of PP-3-T's adsorption behavior to the Langmuir model holds significance, signifying a barrier layer adsorption process where molecules occupy specific sites on the metal surface, forming a protective layer. The consistency of the model with real-world observations validates the assumptions of reversibility and equilibrium between adsorbed and unadsorbed species. DFT-calculated parameters provide molecular-level insights into the corrosion inhibition mechanism of PP-3-T. Parameters such as E_{HOMO}, E_{LUMO}, hardness (η), electronegativity (χ), and ΔN collectively illuminate the inhibitor's reactivity, electron-donating/accepting ability, and potential for charge transfer. These parameters align well with the experimental data, confirming the molecule's suitability for adsorption onto the metal surface. The combination of experimental findings, adherence to the Langmuir model, and insights from DFT calculations strengthens our comprehension of PP-3-T's corrosion inhibition mechanism, paving the way for further studies. These insights offer a comprehensive understanding of the inhibition mechanism, supporting its practical application in corrosion control.

5. Conclusion

In this study, we conducted an investigation into the corrosion inhibition properties of PP-3-T for mild steel in hydrochloric acid (HCl) solution. By integrating experimental measurements, quantum chemical calculations, and theoretical models, we aimed to elucidate the mechanism underlying PP-3-T's effectiveness as a corrosion inhibitor. Our findings reveal several key insights. Experimental data demonstrate a significant improvement in corrosion resistance with the presence of PP-3-T, achieving an inhibition efficiency of up to 96.1%. Importantly, this inhibition efficiency remains consistent across varying PP-3-T concentrations, immersion times, and temperatures. While the adherence to the Langmuir adsorption model suggests the formation of a barrier layer, we acknowledge

that this interpretation may be subject to assumptions and theoretical predictions. DFT-calculated parameters provide additional insights into PP-3-T's corrosion inhibition potential by elucidating its electron-donating/accepting abilities and charge distribution. PP-3-T exhibits potent efficacy as a corrosion inhibitor for mild steel in HCl solution, underscoring its stability and practical applicability. The adsorption mechanism, driven by chemisorption and facilitated by the high negative charges of oxygen and nitrogen atoms, supports the molecule's protective nature on the metal surface. The implications of our research extend to corrosion mitigation strategies across industries. PP-3-T's demonstrated ability to form a protective barrier against corrosive environments presents a promising avenue for developing corrosion-resistant coatings and treatments. Moreover, achieving high inhibition efficiencies at relatively low concentrations of PP-3-T signifies its economic feasibility for large-scale applications. While our study provides valuable insights, opportunities for further research exist. Investigating the long-term stability of the PP-3-T protective layer under extended exposure to aggressive environments could offer insights into its durability.

References

1. M.M. Solomon, I.E. Uzoma, J.A.O. Olugbuyiro and O.T. Ademosun, A Censorious Appraisal of the Oil Well Acidizing Corrosion Inhibitors, *J. Pet. Sci. Eng*., 2022, **215**, 110711. doi: 10.1016/j.petrol.2022.110711
2. D. Wang, Y. Li, B. Chen and L. Zhang, Novel Surfactants as Green Corrosion Inhibitors for Mild Steel in 15% HCl: Experimental and Theoretical Studies, *Chem. Eng. J*., 2020, **402**, 126219. doi: 10.1016/j.cej.2020.126219
3. B. El-Haitout, I. Selatnia, H. Lgaz, M.R. Al-Hadeethi, H.S. Lee, A. Chaouiki, Y.G. Ko, I.H. Ali and R. Salghi, Exploring the Feasibility of New Eco-Friendly Heterocyclic Compounds for Establishing Efficient Corrosion Protection for N80 Steel in a Simulated Oil Well Acidizing Environment: From Molecular-Level Prediction to Experimental Validation, *Colloids Surf., A*, 2023, **656**, 130372. doi: 10.1016/j.colsurfa.2022.130372
4. B.D.B. Tiu and R.C. Advincula, Polymeric Corrosion Inhibitors for the Oil and Gas Industry: Design Principles and Mechanism, *React. Funct. Polym*., 2015, **95**, 25–45. doi: 10.1016/j.reactfunctpolym.2015.08.006
5. A.H. Alamri, Localized Corrosion and Mitigation Approach of Steel Materials Used in Oil and Gas Pipelines – An Overview, *Eng. Failure Anal*., 2020, **116**, 104735. doi: 10.1016/j.engfailanal.2020.104735
6. D.S. Chauhan, M.A.J. Mazumder, M.A. Quraishi and K.R. Ansari, Chitosan Cinnamaldehyde Schiff Base: A Bioinspired Macromolecule as Corrosion Inhibitor for Oil and Gas Industry, *Int. J. Biol. Macromol*., 2020, **158**, 127–138. doi: 10.1016/j.ijbiomac.2020.04.200
7. S. Şafak, B. Duran, A. Yurt and G. Türkoğlu, Schiff Bases as Corrosion Inhibitor for Aluminium in HCl Solution, *Corros. Sci*., 2012, **54**, 251–259. doi: 10.1016/j.corsci.2011.09.026

8. F.E.T. Heakal and A.E. Elkholy, Gemini Surfactants as Corrosion Inhibitors for Carbon Steel, *J. Mol. Liq*., 2017, **230**, 395–407. doi: 10.1016/j.molliq.2017.01.047
9. M. Farsak, H. Keleş and M.A. Keleş, New Corrosion Inhibitor for Protection of Low Carbon Steel in HCl Solution, *Corros. Sci*., 2015, **98**, 223–232. doi: 10.1016/j.corsci.2015.05.036
10. R.G. Parr and R.G. Pearson, Absolute Hardness: Companion Parameter to Absolute Electronegativity, *J. Am. Chem. Soc*., 1983, **105**, no. 26, 7512–7516. doi: 10.1021/ja00364a005
11. T.K. Chaitra, K.N.S. Mohana and H.C. Tandon, Thermodynamic, Electrochemical and Quantum Chemical Evaluation of Some Triazole Schiff Bases as Mild Steel Corrosion Inhibitors in Acid Media, *J. Mol. Liq*., 2015, **211**, 1026–1038. doi: 10.1016/j.molliq.2015.08.031
12. L.A. Khamaza, Generalized Diagram of the Ultimate Nominal Stresses (Endurance Limit) and the Corresponding Dimensions of the Non-Propagating Fatigue Cracks for Sharp and Blunt Notches, *Strength Mater*., 2019, **51**, 350–360. doi: 10.1007/s11223-019-00081-w
13. Yu.G. Matvienko, Approaches of Fracture Mechanics in the Analysis of Admissible Defects in the Form of Notches, *Strength Mater*., 2010, **42**, 58–63. doi: 10.1007/s11223-010-9188-2
14. D. Dwivedi, K. Lepková and T. Becker, Carbon steel corrosion: a review of key surface properties and characterization methods, *RSC Adv*., 2017, **7**, 4580–4610. doi: 10.1039/C6RA25094G
15. D.A. Winkler, Predicting the performance of organic corrosion inhibitors, *Metals*, 2017, **7**, no. 12, 553. doi: 10.3390/met7120553
16. C. Verma, L.O. Olasunkanmi, E.E. Ebenso and M.A. Quraishi, Substituents effect on corrosion inhibition performance of organic compounds in aggressive ionic solutions: a review, *J. Mol. Liq*., 2018, **251**, 100–118. doi: 10.1016/j.molliq.2017.12.055
17. O. Kaczerewska, R. Leiva-Garcia, R. Akid, B. Brycki, I. Kowalczyk and T. Pospieszny, Heteroatoms and π electrons as favorable factors for efficient corrosion protection, *Mater. Corros*., 2019, **70**, no. 6, 1099–1110. doi: 10.1002/maco.201810570
18. D.K. Verma, Y. Dewangan, A.K. Dewangan and A. Asatker, Heteroatom-Based Compounds as Sustainable Corrosion Inhibitors: An Overview, *J. Bio Tribo Corros*., 2021, **7**, no. 15, 1–18. doi: 10.1007/s40735-020-00447-7
19. M. Athar, H. Ali and M.A. Quraishi, Corrosion inhibition of carbon steel in hydrochloric acid by organic compounds containing heteroatoms, *Br. Corros. J*., 2002, **37**, no. 2, 155–158. doi: 10.1179/000705902225002376
20. S. Hadisaputra, A.A. Purwoko, I. Ilhamsyah, S. Hamdiani, D. Suhendra, N. Nuryono and B. Bundjali, A combined experimental and theoretical study of (*E*)-ethyl 3-(4-methoxyphenyl) acrylate as corrosion inhibitor of iron in 1 M HCl solutions, *Int. J. Corros. Scale Inhib*., 2018, **7**, no. 4, 633–647. doi: 10.17675/2305-6894-2018-7-4-10

21. S. Hadisaputra, A.A. Purwoko, Rahmawati, D. Asnawati, Ilhamsyah, S. Hamdiani and Nuryono, Experimental and Theoretical Studies of (2R)-5-hydroxy-7-methoxy-2-phenyl-2,3- dihydrochromen-4-one as corrosion inhibitor for Iron in Hydrochloric Acid, *Int. J. Electrochem. Sci*., 2019, **14**, no. 12, 11110–11121. doi: 10.20964/2019.12.77
22. ASTM International, *Standard Practice for Preparing, Cleaning, and Evaluating Corrosion Test*, 2011, 1–9.
23. S.S. Hadisaputra, A.A. Purwoko, A. Hakim, R. Wati, D. Asnawati and Y.P. Prananto, Experimental and Theoretical Study of Pinostrobin as Copper Corrosion Inhibitor at 1 M H_2SO_4 Medium, *IOP Conf. Ser.: Mater. Sci. Eng*., 2020, **833**, no. 012010. doi: 10.1088/1757-899X/833/1/012010
24. E.D. Akpan, A.K. Singh, H. Lgaz, T.W. Quadri, S.K. Shukla, B. Mangla, A. Dwivedi, O. Dagdag, E.E. Inyang and E.E. Ebenso, Coordination compounds as corrosion inhibitors of metals: A review, *Coord. Chem. Rev*., 2024, **499**, 215503. doi: 10.1016/j.ccr.2023.215503
25. S. Hadisaputra, A.A. Purwoko, F. Wajdi, I. Sumarlan and S. Hamdiani, Theoretical study of the substituent effect on corrosion inhibition performance of benzimidazole and its derivatives, *Int. J. Corros. Scale Inhib*., 2019, **8**, no. 3, 673–688. doi: 10.17675/2305-6894-2019-8-3-15
26. NACE International, *Laboratory Corrosion Testing of Metals in Static Chemical Cleaning Solutions at Temperatures below 93°C (200°F)*, TM0193-2016-SG, 2000.
27. A. Al-Amiery, Anti-corrosion performance of 2-isonicotinoyl-nphenylhydrazinecarbothioamide for mild steel hydrochloric acid solution: Insights from experimental measurements and quantum chemical calculations, *Surf. Rev. Lett*., 2021, **28**, no. 3, 2050058. doi: 10.1142/S0218625X20500584
28. A.A. Alamiery, Investigations on corrosion inhibitory effect of newly quinoline derivative on mild steel in HCl solution complemented with antibacterial studies, *Biointerface Res. Appl. Chem*., 2022, **12**, no. 2, 1561–1568. doi: 10.33263/BRIAC122.15611568
29. V.C. Anadebe, V.I. Chukwuike, K.C. Nayak, E.E. Ebenso and R.C. Barik, Combined electrochemical, atomic scale-DFT and MD simulation of Nickel based metal organic framework (Ni-MOF) as corrosion inhibitor for X65 pipeline steel in CO_2-saturated brine, *Mater. Chem. Phys*., 2024, **312**, 128606. doi: 10.1016/j.matchemphys.2023.128606
30. A. Alamiery, W.N.R.W. Isahak, H. Aljibori, H. Al-Asadi and A. Kadhum, Effect of the structure, immersion time and temperature on the corrosion inhibition of 4-pyrrol-1-yl-*N*-(2,5-dimethyl-pyrrol-1-yl)benzoylamine in 1.0 m HCl solution, *Int. J. Corros. Scale Inhib*., 2021, **10**, no. 2, 700–713. doi: 10.17675/2305-6894-2021-10-2-14
31. A. Alamiery, E. Mahmoudi and T. Allami, Corrosion inhibition of low-carbon steel in hydrochloric acid environment using a Schiff base derived from pyrrole: gravimetric and computational studies, *Int. J. Corros. Scale Inhib*., 2021, **10**, no. 2, 749–765. doi: 10.17675/2305-6894-2021-10-2-17

32. A.J.M. Eltmimi, A. Alamiery, A.J. Allami, R.M. Yusop, A.H. Kadhum and T. Allami, Inhibitive effects of a novel efficient Schiff base on mild steel in hydrochloric acid environment, *Int. J. Corros. Scale Inhib*., 2021, **10**, no. 2, 634–648. doi: 10.17675/2305-6894-2021-10-2-10
33. M.J. Frisch, G.W. Trucks, H.B. Schlegel, G.E. Scuseria, M.A. Robb, J.R. Cheeseman, J.A. Montgomery, Jr., T. Vreven, K.N. Kudin, J.C. Burant, J.M. Millam, S.S. Iyengar, J. Tomasi, V. Barone, B. Mennucci, M. Cossi, G. Scalmani, N. Rega, G.A. Petersson, H. Nakatsuji, M. Hada, M. Ehara, K. Toyota, R. Fukuda, J. Hasegawa, M. Ishida, T. Nakajima, Y. Honda, O. Kitao, H. Nakai, M. Klene, X. Li, J.E. Knox, H.P. Hratchian, J.B. Cross, V. Bakken, C. Adamo, J. Jaramillo, R. Gomperts, R.E. Stratmann, O. Yazyev, A.J. Austin, R. Cammi, C. Pomelli, J.W. Ochterski, P.Y. Ayala, K. Morokuma, G.A. Voth, P. Salvador, J.J. Dannenberg, V.G. Zakrzewski, S. Dapprich, A.D. Daniels, M.C. Strain, O. Farkas, D.K. Malick, A.D. Rabuck, K. Raghavachari, J.B. Foresman, J.V. Ortiz, Q. Cui, A.G. Baboul, S. Clifford, J. Cioslowski, B.B. Stefanov, G. Liu, A. Liashenko, P. Piskorz, I. Komaromi, R.L. Martin, D.J. Fox, T. Keith, M.A. Al-Laham, C.Y. Peng, A. Nanayakkara, M. Challacombe, P.M.W. Gill, B. Johnson, W. Chen, M.W. Wong, C. Gonzalez and J.A. Pople, *Gaussian 03, Revision B. 05*, Gaussian, Inc., Wallingford, CT, 2004.
34. T. Koopmans, Ordering of wave functions and eigen-energies to the individual electrons of an atom, *Physica*, 1934, **1**, no. 1–6, 104–113 (in German). doi: 10.1016/S0031-8914(34)90011-2
35. X. Wang, J. Liu, Z. Zhang, Q. Xiang, J. Zhang, L. Chen and H. Xie, Mechanism for corrosion inhibition of pure iron in 1 M HCl by *Rauiella Fujisana*: Experimental, GCMS, DFT, VASP and solidliquid modeling studies, *Ind. Crops Prod*., 2024, **207**, 117692. doi: 10.1016/j.indcrop.2023.117692
36. A. Singh, A. Pandey, P. Banerjee, S. Saha, B. Chugh, S. Thakur, B. Pani, P. Chaubey and G. Singh, Eco-Friendly Disposal of Expired Anti-Tuberculosis Drug Isoniazid and Its Role in the Protection of Metal, *J. Environ. Chem. Eng*., 2019, **7**, no. 2, 102971. doi: 10.1016/j.jece.2019.102971
37. M.S. Abdulazeez, Z.S. Abdullahe, M.A. Dawood, Z.K. Handel, R.I. Mahmood, S. Osamah, A.H. Kadhum, L.M. Shaker and A.A. Al-Amiery, Corrosion inhibition of low carbon steel in HCl medium using a thiadiazole derivative: weight loss, DFT studies and antibacterial studies, *Int. J. Corros. Scale Inhib*., 2021, **10**, no. 4, 1812–1828. doi: 10.17675/2305-6894-2021-10-4-27
38. K. Cao, W. Li and L. Yu, Investigation of 1-Phenyl-3-Methyl-5-Pyrazolone as a corrosion inhibitor for mild steel in 1 M hydrochloric acid, *Int. J. Electrochem. Sci*., 2012, **7**, 806–818.
39. A.Z. Salman, Q.A. Jawad, K.S. Ridah, L.M. Shaker and A.A. Al-Amiery, Selected BISThiadiazole: Synthesis and Corrosion Inhibition Studies on Mild Steel in HCl Environment, *Surf. Rev. Lett*., 2020, **27**, no. 12, 2050014. doi: 10.1142/S0218625X20500146

40. A. Fouda, A. Al-Sarawy and E. El-Katori, Thiazole derivatives as corrosion inhibitors for C-steel in sulphuric acid solution, *Eur. J. Chem*., 2010, **1**, no. 4, 312–318. doi: 10.5155/eurjchem.1.4.312-318.105
41. M. Benabdellah, A. Tounsi, K. Khaled and B. Hammouti, Thermodynamic, Chemical and Electrochemical Investigations of 2-Mercapto Benzimidazole as Corrosion Inhibitor for Mild Steel in Hydrochloric Acid Solutions, *Arabian J. Chem*., 2011, **4**, no. 1, 17–24. doi: 10.1016/j.arabjc.2010.06.010
42. R. Haldhar, D. Prasad, A. Saxena and P. Singh, *Valeriana Wallichii* Root Extract as a Green & Sustainable Corrosion Inhibitor for Mild Steel in Acidic Environments: Experimental and Theoretical, *Mater. Chem. Front*., 2018, **2**, no. 6, 1225–1237. doi: 10.1039/C8QM00120K
43. A.K. Singh, S. Shukla and E. Ebenso, Cefacetrile as Corrosion Inhibitor for Mild Steel in Acidic Media, *Int. J. Electrochem. Sci*., 2011, **6**, no. 11, 5689–5700. doi: 10.1016/S1452-3981(23)18437-9
44. A. Alamiery, A. Mohamad, A. Kadhum and M. Takriff, Comparative data on corrosion protection of mild steel in HCl using two new thiazoles, *Data Brief*, 2022, **40**, 107838. doi: 10.1016/j.dib.2022.107838
45. Y. Zhang, Y. Cheng, F. Ma and K. Cao, Corrosion Inhibition of Carbon Steel by 1-Phenyl-3-Amino-5-Pyrazolone in H_2SO_4 solution, *Int. J. Electrochem. Sci*., 2019, **14**, no. 1, 999–1008. doi: 10.20964/2019.01.69
46. A.S. Fouda, A.A. Al-Sarawy and E.E. El-Katori, Pyrazolone derivatives as corrosion inhibitors for C-steel in hydrochloric acid solution, *Desalination*, 2006, **201**, 1–13. doi: 10.1016/j.desal.2006.03.519
47. S. Hadisaputra, A.A. Purwoko, A. Hakim, L.R.T. Savalas, R. Rahmawati, S. Hamdiani and N. Nuryono, Ab initio MP2 and DFT studies of ethyl-p-methoxycinnamate and its derivatives as corrosion inhibitors of iron in acidic medium, *J. Phys.: Conf. Ser*., 2019, **1402**, 055046. doi: 10.1088/1742-6596/1402/5/055046
48. V.S. Sastri and J.R. Perumareddi, Molecular orbital theoretical studies of some organic corrosion inhibitors, *Corrosion*, 1997, **53**, no. 8, 617–622. doi: 10.5006/1.3290294
49. G.F. de Sousa, C.C. Gatto, I.S. Resck and V.M. Deflon, Synthesis, spectroscopic studies and X-ray Crystal structures of new pyrazoline and pyrazole derivatives, *J. Chem. Crystallogr*., 2011, **41**, 401–408. doi: 10.1007/s10870-010-9896-2
50. S. Hadisaputra, Z. Iskandar and D. Asnawati, Prediction of the Corrosion Inhibition Efficiency of Imidazole Derivatives: A Quantum Chemical Study, *Acta Chim. Asiana*, 2019, **2**, no. 1, 88–94. doi: 10.29303/aca.v2i1.15
51. N.O. Eddy, S.R. Stoyanov and E.E. Ebenso, Fluoroquinolones as corrosion inhibitors for mild steel in acidic medium; experimental and theoretical studies, *Int. J. Electrochem. Sci*., 2010, **5**, no. 8, 1127–1150.
52. Y. Wirayani, M. Ulfa and Y. Yahmin, Corrosion inhibition efficiency of nicotine based on quantum chemical study, *Acta Chim. Asiana*, 2018, **1**, no. 2, 37–42. doi: 10.29303/aca.v1i2.29

53. A.S. Fouda, M.A. Ismail, A.S. Abousalem and G.Y. Elewady, Experimental and theoretical studies on corrosion inhibition of 4-amidinophenyl-2,2'-bifuran and its analogues in acidic media, *RSC Adv.*, 2017, **7**, 46414–46430. doi: 10.1039/C7RA08092A
54. K.S. Bokati, and C. Dehghanian, Adsorption behavior of 1H-benzotriazole corrosion inhibitor on aluminum alloy 1050, mild steel and copper in artificial seawater, *J. Environ. Chem. Eng.*, 2018, **6**, no. 2, 1613–1624. doi: 10.1016/j.jece.2018.02.015
55. M. Mahdavian and S. Ashhari, Corrosion inhibition performance of 2-mercaptobenzimidazole and 2-mercaptobenzoxazole compounds for protection of mild steel in hydrochloric acid solution, *Electrochim. Acta*, 2010, **55**, no. 1, 1720–1724. doi: 10.1016/j.electacta.2009.10.055
56. S. Ahmadi and A. Khormali, Optimization of the corrosion inhibition performance of 2-mercaptobenzothiazole for carbon steel in HCl media using response surface methodology, *Fuel*, 2024, **357**, 129783. doi: 10.1016/j.fuel.2023.129783
57. S.A. Abd El-Maksoud and A.S. Fouda, Some pyridine derivatives as corrosion inhibitors for carbon steel in acidic medium, *Mater. Chem. Phys*., 2005, **93**, no. 1, 84–90. doi: 10.1016/j.matchemphys.2005.02.020
58. O. Krim, A. Elidrissi, B. Hammouti, A. Ouslim and M. Benkaddour, Synthesis, characterization, and comparative study of pyridine derivatives as corrosion inhibitors of mild steel in HCl medium, *Chem. Eng. Commun*., 2009, **96**, no. 12, 1536–1546. doi: 10.1080/00986440903155451
59. K.R. Ansari, M.A. Quraishi and A. Singh, Pyridine derivatives as corrosion inhibitors for N80 steel in 15% HCl: Electrochemical, surface and quantum chemical studies, *Measurement*, 2015, **76**, 136–147. doi: 10.1016/j.measurement.2015.08.028
60. K.R. Ansari, M.A. Quraishi and A. Singh, Corrosion inhibition of mild steel in hydrochloric acid by some pyridine derivatives: an experimental and quantum chemical study, *J. Ind. Eng. Chem*., 2015, **25**, 89–98. doi: 10.1016/j.jiec.2014.10.017
61. A.A. Farag, E.A. Mohamed, G.H. Sayed and K.E. Anwer, Experimental/computational assessments of API steel in 6 M H_2SO_4 medium containing novel pyridine derivatives as corrosion inhibitors, *J. Mol. Liq*., 2021, **330**, 115705. doi: 10.1016/j.molliq.2021.115705
62. A.A. Al-Amiery, W.N.R.W. Isahak and W.K. Al-Azzawi, Corrosion Inhibitors: Natural and Synthetic Organic Inhibitors, *Lubricants*, 2023, **11**, 174. doi: 10.3390/lubricants11040174
63. N.M. El Basiony, T. Tawfik, M.A. El-Raouf, A.A. Fadda and M.M. Waly, Synthesis, characterization, theoretical calculations (DFT and MC), and experimental of different substituted pyridine derivatives as corrosion mitigation for X-65 steel corrosion in 1M HCl, *J. Mol. Struct*., 2021, **1231**, 129999. doi: 10.1016/j.molstruc.2021.129999
64. A. Alrebh, M.B. Rammal and S. Omanovic, A pyridine derivative 2-(2-Methylaminoethyl)pyridine (MAEP) as a ‘green’ corrosion inhibitor for low-carbon steel in hydrochloric acid media, *J. Mol. Struct.*, 2021, **1238**, 130333. doi: 10.1016/j.molstruc.2021.130333

65. O. El Khattabi, B. Zerga, M. Sfaira, M. Taleb, M. Ebn Touhami, B. Hammouti, L. Herrag and M. Mcharfi, On the adsorption properties of an imidazole-pyridine derivative as corrosion inhibitor of mild steel in 1 M HCl, *Pharma Chem*., 2021, **4**, 1759–1768.
66. M.A. Dawood, Z.M.K. Alasady, M.S. Abdulazeez, D.S. Ahmed, G.M. Sulaiman, A.A.H. Kadhum, L.M. Shaker and A.A. Alamiery, The corrosion inhibition effect of a pyridine derivative for low carbon steel in 1 M HCl medium: Complemented with antibacterial studies, *Int. J. Corros. Scale Inhib*., 2021, **10**, no. 4, 1766–1782. doi: 10.17675/2305-6894-2021-10-4-25
67. A. Ghazoui, R. Saddik, N. Benchat, M. Guenbour, B. Hammouti, S.S. Al-Deyab and A. Zarrouk, Comparative study of pyridine and pyrimidine derivatives as corrosion inhibitors of C38 steel in molar HCl, *Int. J. Electrochem. Sci*., 2012, **7**, no. 8, 7080–7097. doi: 10.1016/S1452-3981(23)15769-5
68. T.K. Chaitra, K.N. Mohana and H.C. Tandon, Study of new thiazole based pyridine derivatives as potential corrosion inhibitors for mild steel: theoretical and experimental approach, *Int. J. Corros*., 2016, **2016**. doi: 10.1155/2016/9532809
69. A. Saady, Z. Rais, F. Benhiba, R. Salim, K. Ismaily Alaoui, N. Arrousse, F. Elhajjaji, M. Taleb, K. Jarmoni, Y. Kandri Rodi, I. Warad and A. Zarrouk, Chemical, electrochemical, quantum, and surface analysis evaluation on the inhibition performance of novel imidazo[4,5-b] pyridine derivatives against mild steel corrosion, *Corros. Sci*., 2021, **189**, no. 10, 109621. doi: 10.1016/j.corsci.2021.109621
70. A. Singh, K.R. Ansari, I.H. Ali, A.K. Alanazi, M. Younas and Y. Lin, Long chain imidazole derivative as a novel corrosion inhibitor for Q235 steel in 15% HCl medium under hydrodynamic condition: Experimental and theoretical examinations, *Mater. Chem. Phys*., 2024, 128798. doi: 10.1016/j.matchemphys.2023.128798
71. R.A. El-Nagar, N.A. Khalil, Y. Atef, M.I. Nessim and A. Ghanem, Evaluation of ionic liquids based imidazolium salts as an environmentally friendly corrosion inhibitors for carbon steel in HCl solutions, *Sci. Rep*., 2024, **14**, no. 1, 1889. doi: 10.1038/s41598-024-52174-5
72. W. Ettahiri, M. Adardour, E. Ech-chihbi, M. Azam, R. Salim, S. Dalbouha, K. Min, Z. Rais, A. Baouid and M. Taleb, 1,2,3-triazolyl-linked benzimidazolone derivatives as new eco-friendly corrosion inhibitors for mild steel in 1 M HCl solution: Experimental and computational studies, *Colloids Surf., A*, 2024, **681**, 132727. doi: 10.1016/j.colsurfa.2023.132727
73. N. Kedimar, P. Rao and S.A. Rao, Imidazole-based ionic liquid as a corrosion inhibitor for aluminum alloy and it's composite in HCl – A comparative study, *Inorg. Chem. Commun*., **160**, 2024, 112020. doi: 10.1016/j.inoche.2024.112020

74. R.L. Camacho-Mendoza, E. Gutiérrez-Moreno, E. Guzmán-Percástegui, E. Aquino-Torres, J. Cruz-Borbolla, J.A. Rodríguez-Ávila, J.G. Alvarado-Rodríguez, O. Olvera-Neria, P. Thangarasu and J.L. Medina-Franco, Density functional theory and electrochemical studies: structure–efficiency relationship on corrosion inhibition, *J. Chem. Inf. Model*., 2015, **55**, 2391–2402. doi: 10.1021/acs.jcim.5b00385
75. K. Jrajri, F. Benhiba, M. Oubaaqa, S. Safi, A. Zaroual, M. El Moudane, I. Warad, D.R. Bazanov, N.A. Lozinskaya, A. Bellaouchou, A. Zarrouk, Electrochemical, surface and theoretical investigations of a new tri-tolyl imidazole designed for corrosion inhibition of carbon steel in normal hydrochloric acid medium, *Inorg. Chem. Commun*., 2023, **157**, 111309. doi: 10.1016/j.inoche.2023.111309
76. P. Wang, L. Fan, Y. Song, K. Deng, L. Guo, Z. Li, and Y. Lin, Synergistic effect of new imidazoline derivative and 2-aminopyridine as corrosion inhibitors for Q235: Experimental and theoretical study, *Surf. Interface Anal*., 2024. doi: 10.1002/sia.7286

♦ ♦ ♦